CHINESE OPTICS LETTERS

Vol. 22, No. 2 | February 2024

Controllable transitions among phase-matching conditions in a single nonlinear crystal

Ziqi Zeng (曾梓琦)[1,†], Shixin You (尤世欣)[1,†], Zixiang Yang (杨子祥)[1], Chenzhi Yuan (袁晨智)[1], Chenglong You (由成龙)[2], and Ruibo Jin (金锐博)[1*]

[1] Hubei Key Laboratory of Optical Information and Pattern Recognition, Wuhan Institute of Technology, Wuhan 430205, China

[2] Quantum Photonics Laboratory, Department of Physics and Astronomy, Louisiana State University, Baton Rouge, Louisiana 70803, USA

[†]These authors contributed equally to this work.

*Corresponding author: jin@wit.edu.cn

Received July 3, 2023 | Accepted September 25, 2023 | Posted Online February 20, 2024

Entangled photon pairs are crucial resources for quantum information processing protocols. Via the process of spontaneous parametric downconversion (SPDC), we can generate these photon pairs using bulk nonlinear crystals. Traditionally, the crystal is designed to satisfy a specific type of phase-matching condition. Here, we report controllable transitions among different types of phase matching in a single periodically poled potassium titanyl phosphate crystal. By carefully selecting pump conditions, we can satisfy different phase-matching conditions. This allows us to observe first-order Type-II, fifth-order Type-I, third-order Type-0, and fifth-order Type-II SPDCs. The temperature-dependent spectra of our source were also analyzed in detail. Finally, we discussed the possibility of observing more than nine SPDCs in this crystal. Our work not only deepens the understanding of the physics behind phase-matching conditions, but also offers the potential for a highly versatile entangled biphoton source for quantum information research.

Keywords: spontaneous parametric downconversion; nonlinear crystals; phase-matching condition.

DOI: 10.3788/COL202422.021901

1. Introduction

Quantum light sources, including single-photon sources and entangled photon sources, are fundamental resources for the study of quantum information processing[1,2]. One of the most widely used methods for preparing quantum light sources is spontaneous parametric downconversion (SPDC) in a nonlinear optical crystal[3,4]. In an SPDC process, a pump photon interacts with a nonlinear crystal and is converted into a biphoton, which is a pair of correlated photons usually referred to as the signal and idler. The biphotons can be further engineered to prepare a heralded single-photon source or entangled photon source. The SPDC process can be engineered in different degrees of freedom, such as space, time, frequency, polarization, and phase[5,6].

According to the polarization of the pump, signal, and idler photons, the phase-matching conditions in nonlinear SPDC can be classified into three types: Type-0, H→HH, or V→VV; Type-I, H→VV, or V→HH; Type-II, H→HV, or V→HV. Here, "H" and "V" represent the horizontal and vertical polarizations, respectively[7]. In the Type-0 and Type-I cases, the signal and idler photons have the same polarization, resulting in broad spectral distributions and narrow temporal distributions. This feature of broad spectra is advantageous in quantum metrology[8,9], quantum optical coherence tomography[10], and quantum spectroscopy[11,12]. Furthermore, the Type-0 matching condition has the highest effective nonlinear coefficient among all three nonlinear phase-matching conditions[7]. In the Type-II cases, the signal and idler photons usually have much narrower spectra and have been widely used to perform quantum communication, computation, and measurement[13–16]. Another important feature of the Type-II matching condition is that the joint spectral distribution of biphotons can be engineered according to the group velocity differences[17]. As a result, one can prepare photon pair sources with engineerable frequency correlation[5,6,18].

Traditionally, one crystal is usually designed to satisfy only one specific phase-matching condition for quantum information processing protocols. For different protocols, one may need different crystals supporting different phase-matching conditions. Previous works have demonstrated the possibility of realizing two SPDC processes in a single periodically poled potassium titanyl phosphate (PPKTP) crystal. These studies were limited to only Type-II and Type-0 phase-matching conditions, and the detailed properties of such sources are unclear[19–22]. In this work, we demonstrate controllable transitions among all types of phase matching in a single nonlinear

crystal. Specifically, we find that PPKTP with a poling period of 10 μm can realize all three types of phase-matching conditions simultaneously at pump wavelengths of around 405 nm. We observed first-order Type-II (at 404.3 nm), fifth-order Type-I (at 404.3 nm), third-order Type-0 (at 408.8 nm), and fifth-order Type-II (at 315 nm) phase-matching conditions. More importantly, the design principles, detailed spectra, and tuning curves in our sources are revealed for future reference. Our work may provide a versatile biphoton source for diverse tasks in quantum information technology.

2. Theory

In the process of an SPDC, the energy conservation law is satisfied and is given as

$$\omega_p = \omega_s + \omega_i, \tag{1}$$

where ω is the angular frequency and the subscripts p, s, and i denote the pump, signal, and idler, respectively. The momentum conservation law is also satisfied and can be expressed in the form of phase-matching function (PMF). For quasi-phase-matched (QPM) crystals, the PMF is given by

$$k_p - k_s - k_i \pm m\frac{2\pi}{\Lambda} = 0, \tag{2}$$

where k_j $(j = p, s, i)$ is the wave vector, Λ is the poling period, and $m = 1, 3, 5\ldots$ is the poling order.

In a PPKTP crystal, the photons are usually designed to propagate along the x direction but polarize in the y and z directions. Here, we assign y direction to H polarization and z direction to V polarization. Using the Sellmeier equations of KTP from Ref. [23] for refractive index n_y, Ref. [24] for n_z, and Ref. [25] for temperature-dependent dispersion, the PMF in Eq. (2) can be calculated.

In Fig. 1(a), we show the relation between pump wavelength and poling period with nine different combinations of poling order and phase-matching type. Table 1 shows the specific wavelength values of the cross points in Fig. 1(a). Notably, there are three SPDC processes near the wavelength of 405 nm. We inspect these three phase-matching conditions further in Fig. 1(b) by zooming in the wavelength range between 400 and 410 nm. We can confirm that the cross points are at the pump wavelengths of 401.9 nm (third-order Type-0), 404.6 nm (first-order Type-II), and 407.4 nm (fifth-order Type-I). This feature allows us to achieve a controllable transition among Type-0, Type-I, and Type-II phase matching conditions by tuning the pump wavelength in a small range between 401 and 408 nm. Moreover, we can adjust the cross points by tuning the temperature of the PPKTP crystal. Finally, we note that our calculation indicates the existence of another experimentally implementable SPDC process of fifth-order Type-II at 311.4 nm, as shown in Fig. 1(a).

The effective nonlinear coefficient is an important parameter for QPM crystals, which could be different for phase-matching conditions of different types and orders. We define d_{eff} as the effective nonlinear coefficient of KTP and $d(z)$ as the nonlinear coefficient of PPKTP at the position of z. $d(z)$ is a square-wave function[26–28],

$$d(z) = d_{\text{eff}}\ \text{sign}[\cos(2\pi z/\Lambda)]. \tag{3}$$

$d(z)$ can also be expressed by Fourier series,

$$d(z) = d_{\text{eff}} \sum_{m=-\infty}^{\infty} G_m\ \exp(ik_m z), \tag{4}$$

where $k_m = 2\pi m/\Lambda$, and G_m can be expressed as

$$G_m = \left(\frac{2}{m\pi}\right)\sin\left(\frac{m\pi}{2}\right). \tag{5}$$

Intuitively speaking, k_m is the spatial frequency of the grating structure of the PPKTP crystal, and G_m is the coefficient of its

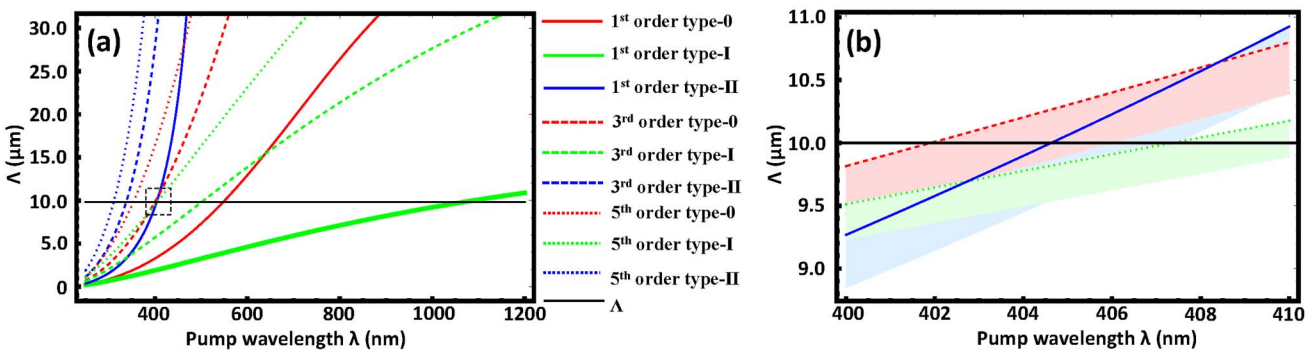

Fig. 1. Calculated poling period of the PPKTP crystal as a function of pump wavelength under different phase-matching conditions. The black horizontal line represents the 10 μm poling period. In this calculation, we assume the degenerate case of $\lambda_s = \lambda_i = 2\lambda_p$, and the temperature of the crystal is set at 25°C. As shown in (a), three phase-matching conditions are satisfied near λ_p = 405 nm. In (b), we show a zoomed-in plot for pump wavelengths between 400 and 410 nm. Here, these shadowed regions represent the temperature tuning range of each phase-matching condition. For each region, the upper bound and lower bound are at 25°C and 150°C, respectively.

Table 1. Comparison of the Nine SPDC Processes[a].

Poling Order	Phase-Matching	Polarization	Pump (nm)	Signal (nm)	Idler (nm)	$d(z)$ (pm/V)	Λ (μm)
First	Type-0	$Z \rightarrow ZZ$	550.82	1101.65	1101.65	$2d_{33}/\pi = 10.76$	
	Type-I	$Z \rightarrow YY$	1070.91	2141.82	2141.82	$2d_{32}/\pi = 2.77$	
	Type-II	$Y \rightarrow YZ$	404.63	809.27	809.27	$2d_{24}/\pi = 2.32$	
Third	Type-0	$Z \rightarrow ZZ$	401.92	803.84	803.84	$2d_{33}/3\pi = 3.59$	
	Type-I	$Z \rightarrow YY$	505.21	1010.41	1010.41	$2d_{32}/3\pi = 0.92$	10
	Type-II	$Y \rightarrow YZ$	338.73	677.45	677.45	$2d_{24}/3\pi = 0.77$	
Fifth	Type-0	$Z \rightarrow ZZ$	354.97	709.94	709.94	$2d_{33}/5\pi = 2.15$	
	Type-I	$Z \rightarrow YY$	407.37	814.73	814.73	$2d_{32}/5\pi = 0.55$	
	Type-II	$Y \rightarrow YZ$	311.43	622.86	622.86	$2d_{24}/5\pi = 0.46$	

[a]$d(z)$ is the theoretical nonlinear coefficient and Λ is the poling period.

eigenmode $\exp(ik_m z)$. The detailed derivation of $d(z)$ and G_m can be found in the Appendices A and B.

3. Experiment and Results

We experimentally verified the existence of these controllable transitions of phase-matching conditions using the experimental setup shown in Fig. 2. We have used two lasers as our pump. The first laser is a narrowband laser (Kunteng QTechnics) with tunable center wavelengths of 401–409 nm and a linewidth of 10 MHz. The second laser is a broadband laser[29], which has a strong-power portion at 405 nm and a weak-power portion at around 315 nm. During our experiment, we control the pump power using a half-wave plate (HWP) and a polarizing beam splitter (PBS). By adding another HWP after the PBS, we can also control the polarization of the pump beam. Then the pump laser is filtered by a short-pass filter and then focused by a lens (L1, with a focal length of $f = 50$ mm) onto a temperature-controlled 10-mm-long PPKTP crystal. Our PPKTP crystal has a poling period of 10 μm, which was originally designed for a Type-II phase-matched SPDC at 810 nm. The downconverted biphotons are collimated by the second lens (L2, $f = 50$ mm) and then filtered by a dichroic mirror and a long-pass filter. Then, these biphotons are separated by the PBS and 50:50 fiber beam splitter (FBS), which directs the photons to two avalanche photodiodes (APDs). Finally, we analyze the properties of these SPDC processes using a time-interval analyzer (Picoharp 300, PicoQuant) for single and coincidence counts (CCs). Moreover, the spectra of these biphotons are measured using a single-photon level spectrometer (SP2300, Princeton Instrument).

We report the measured single counts (SCs) and CCs in Table 2. We also plot the experimentally measured spectra in Figs. 3(a)–3(d). For the first-order Type-II case, the pump wavelength is set at 404.3 nm, and the polarization is set to be horizontal. In this case, the signal and idler are separated by the PBS and then coupled into single-mode fibers, which are connected to two APDs. At the spectral degeneracy temperature of 126.8°C, SC and CC are measured to be 1.3 Mcps and

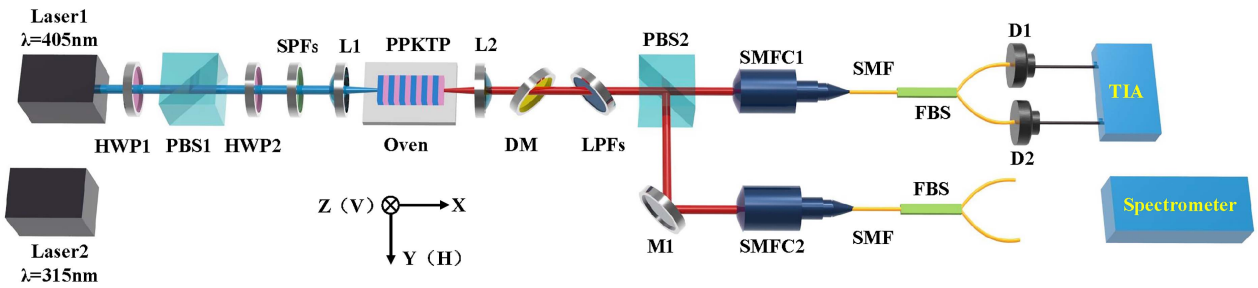

Fig. 2. Experimental setup for observing controllable transitions among different SPDC processes. Here, we used two lasers at 405 and 315 nm. We control the power and polarization of the pump beam, and we also control the temperature of the PPKTP crystal. The properties of these SPDC processes are characterized using a time interval analyzer and a single-photon level spectrometer. HWP, half-wave plate; PBS, polarizing beam splitter; SPFs, short-pass filters; L, lens; DM, dichroic mirror; LPFs, long-pass filters; M, mirror; SMFC, single-mode-fiber coupler; SMF, single-mode fiber; FBS, fiber beam splitter; D, detector.

Table 2. Comparison of the Four SPDC Processes[a].

Poling period		10 μm		
Pump wavelength	404.3 nm	404.3 nm	408.8 nm	315 nm
Phase-matching	Type-II	Type-I	Type-0	Type-II
Polarization	H → H + V	V → H + H	V → V + V	H → H + V
Poling order	1st	5th	3rd	5th
Tuning range	30°C → 150°C	50°C → 70°C	50°C → 120°C	30°C → 150°C
Degenerate temperature	126.8°C	57.2°C	58.4°C	62.8°C
SC/CC (kcps)	1300/45	385/15	5400/167	N/A
Theoretical $d(z)$ (pm/V)	$2d_{24}/\pi = 2.32$	$2d_{32}/5\pi = 0.55$	$2d_{33}/3\pi = 3.59$	$2d_{24}/5\pi = 0.46$

[a]During our characterization, we fixed the pump power to 10 mW. We measure the SC and CC at the degenerate temperature. We note that SC is calculated as $SC = \sqrt{SC1 \times SC2}$, where SC1 and SC2 are the single counts of two different channels. The CC is the original data without correcting the factor of 1/2 in the usage of FBS. Here, $d(z)$ is the nonlinear coefficient of the PPKTP crystal.

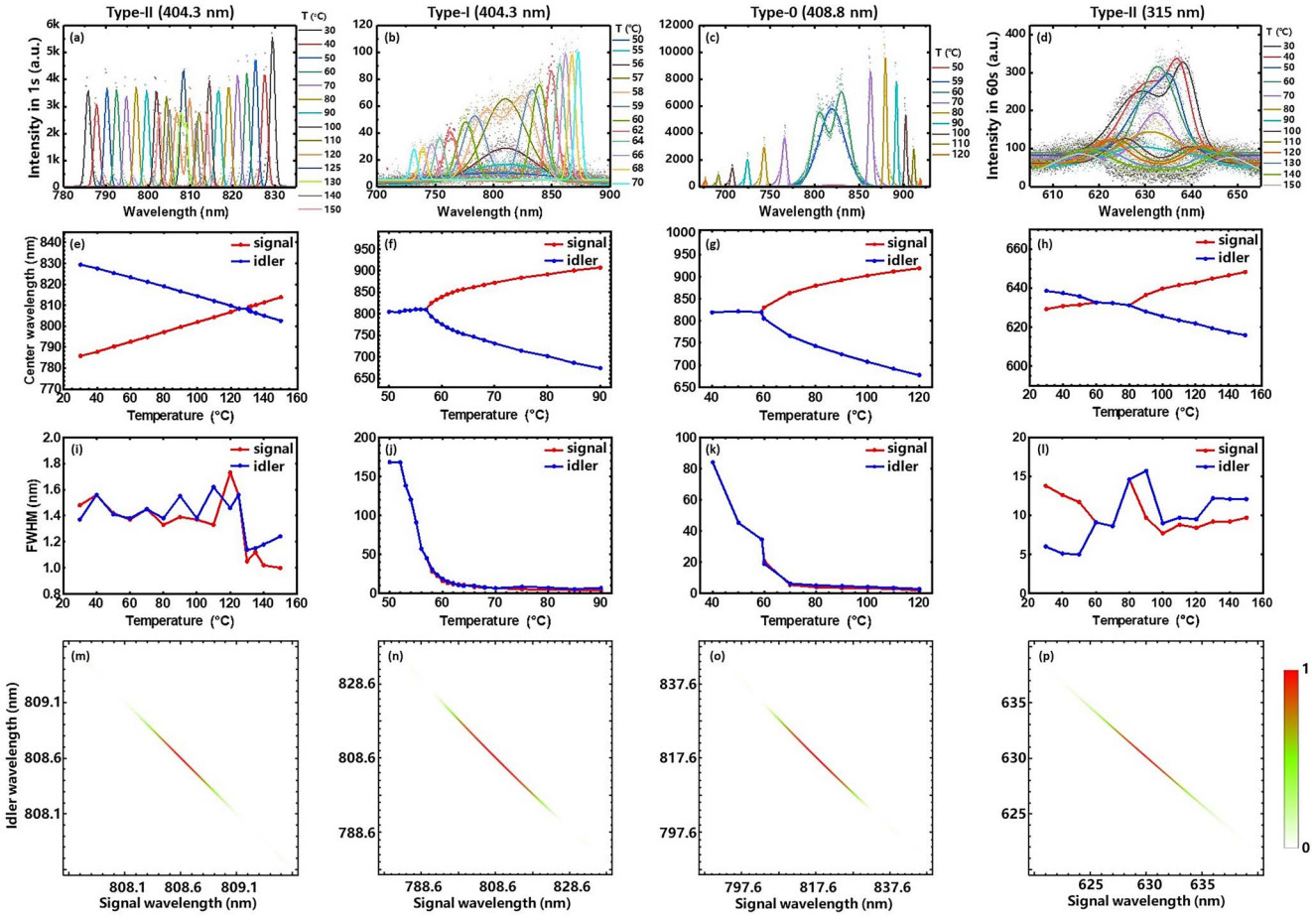

Fig. 3. Measured properties of our versatile biphoton source. (a)–(d) Spectra of the biphotons for different crystal temperatures; (e)–(h) tuning curves of the four observed SPDCs. Here, we report the center wavelengths of the signal and idler photons at different temperatures. (i)–(l) FWHMs of the signal and idler photons at different temperatures. We note that the values in (e)–(l) were obtained by fitting each spectrum to a Gaussian distribution. (m)–(p) Simulated JSIs of the biphotons.

45 kcps (cps, counts per second), respectively. By adjusting the temperature of the crystal from 30°C to 150°C, we measured the spectra shown in Fig. 3(a). The center wavelength of the signal and idler photons, as a function of temperature, also known as the tuning curve, is shown in Fig. 3(e).

For the fifth-order Type-I case, we kept the pump wavelength at 404.3 nm, but we changed the polarization of the pump to vertical. In this case, the signal and idler have the same horizontal polarization (H-polarized). These generated biphotons will transmit through the PBS, and we separate them using a 50:50 FBS to measure the SC and CC. In particular, the measured SC and CC are 385 and 15 kcps at the spectral degeneracy temperature of 57.2°C. By adjusting the temperature from 50°C to 90°C, we measured the spectra shown in Fig. 3(b). The tuning curve is shown in Fig. 3(f), which is clearly different from Fig. 3(e).

For the third-order Type-0 case, the pump wavelength is set to 408.8 nm, and the polarization is set to be vertical. The generated vertically polarized biphotons are reflected by the PBS, collected and separated by another 50:50 FBS, and finally measured by two APDs. At the spectral degeneracy temperature of 58.4°C, the SC and CC are 5.4 Mcps and 167 kcps, respectively. In this case, we tune the temperature of the PPKTP crystal from 50°C to 120°C; we show the measured spectra in Fig. 3(c). The corresponding tuning curve is shown in Fig. 3(g).

In our final measurement, we use a broadband laser with a central wavelength of 315 nm to implement the fifth-order Type-II SPDC process. We note that in this case, the pump power is unknown due to the limitations of our devices. Nevertheless, in this case, the measured spectra and tuning curve are shown in Figs. 3(d) and 3(h). The measured temperature range is 30°C to 150°C, and the spectral degeneracy temperature is measured to be 62.8°C. The observed wavelength of 315 nm slightly deviates from the theoretically calculated value of 311.43 nm, which may indicate that the accuracy of the Sellmeier equation used in the calculations needs further improvement.

As a general observation, we note that the Type-II SPDC has a much narrower FWHM than Type-I and Type-0 SPDC, as also indicated in Figs. 3(i)–3(l).

4. Discussion

To gain a deeper understanding of the biphotons generated under different phase-matching conditions, we calculated the joint spectral intensities (JSIs)[30] under the wavelength degenerate condition, as depicted in Figs. 3(m)–3(p). Notably, the JSIs in Figs. 3(m)–3(o) are distributed along the antidiagonal direction. This is attributed to the narrow spectral width of the pump laser, causing the pump envelope function to predominantly shape the JSI. However, in Fig. 3(p), the JSI deviates from the antidiagonal direction. This discrepancy arises from the broader spectral width of the pump laser, causing the phase-matching function to dominate the JSI.

In this experiment, we only observed four SPDC processes, as listed in Table 2. In the future, it is possible to observe more than nine phase-matching conditions as long as the condition in Eq. (2) is satisfied. Our biphoton source allows for both broadband (Type-0 and Type-I) and narrowband (Type-II) biphoton emission without changing the experimental setup or PPKTP crystal, which is convenient for operations in experiment. In the future, this biphoton source can be upgraded to a polarization-entangled photon source or a time-bin entangled photon source[31,32].

One remarkable finding of this study is the observation of three phase-matching conditions matched within a very short pump wavelength range of 401–408 nm. This wavelength range, particularly around 405 nm, holds significant importance for entangled photon sources, being widely utilized not only in the laboratory[33–35] but also in satellite-based endeavors[36]. The popularity of this wavelength range can be attributed to the maturity of blue-violet laser technology, which allows the production of high-power blue lasers at relatively affordable costs[37–42]. The identification of three phase-matching conditions in this study holds the potential to advance the quantum applications of entangled photon sources utilizing blue lasers and PPKTP crystals.

5. Conclusion

Entangled photon pairs are crucial for quantum information-processing protocols. The possibility of realizing all three types of SPDC processes in a single PPKTP crystal could be beneficial for future research. Here, we experimentally observed four SPDC processes in a single PPKTP crystal with a poling period of 10 μm. These processes include third-order Type-0, first-order Type-II, fifth-order Type-I, and fifth-order Type-II. We have also reported on the properties of these processes, including the CC and thermally dependent spectra. Our scheme can provide a versatile biphoton source for future quantum protocols, as it allows for both broadband (Type-0 and Type-I) and narrowband (Type-II) biphoton sources without changing the experimental setup or PPKTP crystal.

Appendix A: Calculation of d_{eff} for KTP

Here we derive the effective nonlinear coefficient of KTP d_{eff}. In the interaction of strong light with a nonlinear medium, the relationship between the dielectric polarization density $\vec{P}$ and the electric field $\vec{E}$ is nonlinear, and the $\vec{P}$ induced by the medium can be expanded into a power series of $\vec{E}$. We only consider the second-order case[26],

$$\vec{P}(E) = \varepsilon_0 \chi^{(2)} \vec{E}\,\vec{E}, \tag{A1}$$

where ε_0 is the permittivity of free space, $\chi^{(2)}$ is the second-order nonlinear optical susceptibility, and $\vec{E}\,\vec{E}$ is the tensor product of the electrical field. When the Kleiman symmetry condition is

established, $d_{ijk} = \frac{1}{2}\chi^{(2)}_{ijk}$. The nonlinear polarizations of the interacting waves in a PPKTP crystal can be given in the form,

$$\begin{bmatrix} P_x \\ P_y \\ P_z \end{bmatrix} = 2\varepsilon_0 \begin{bmatrix} d_{11} & d_{12} & d_{13} & d_{14} & d_{15} & d_{16} \\ d_{21} & d_{22} & d_{23} & d_{24} & d_{25} & d_{26} \\ d_{31} & d_{32} & d_{33} & d_{34} & d_{35} & d_{36} \end{bmatrix} \begin{bmatrix} E_x^2 \\ E_y^2 \\ E_x^2 \\ 2E_yE_z \\ 2E_xE_z \\ 2E_xE_y \end{bmatrix}, \tag{A2}$$

where P_i $(i = x, y, z)$ is the component of $\vec{P}$ along the x, y, and z axes; d_{ij} $(i = 1\text{–}3; j = 1\text{–}6)$, which is simplified from d_{ijk}, represents the nonlinear susceptibility tensor of the KTP crystal. E_i $(i = 1, 2, 3)$ is the electrical field of the fundamental wave along the x, y, and z axes. For Type-II SPDC, $P_y = \varepsilon_0 d_{24} E_y E_z$, and $d_{\text{eff}} = d_{24}$. For Type-I SPDC, $P_z = \varepsilon_0 d_{32} E_y E_y$, and $d_{\text{eff}} = d_{32}$; for Type-0 SPDC, $P_z = \varepsilon_0 d_{33} E_z E_z$, and $d_{\text{eff}} = d_{33}$. Finally, for PPKTP, $d_{24} = 3.64\,\text{pm/V}$, $d_{32} = 4.35\,\text{pm/V}$, and $d_{33} = 16.9\,\text{pm/V}$[43].

Appendix B: Calculation of Fourier coefficient G_m

Here we derive the Fourier coefficient G_m [Eq. (5)] in the main text. Considering $d(z)$ is a square-wave function,

$$d(z) = d_{\text{eff}}\,\text{sign}[\cos(2\pi z/\Lambda)], \tag{B1}$$

where d_{eff} denotes the nonlinear coefficient of the KTP and Λ is the poling period of PPKTP.

Arbitrary periodic signals that satisfy the Dirichlet conditions[44] can be rewritten as Fourier series in exponential form,

$$f(t) = \sum_{n=-\infty}^{\infty} c_n e^{in\omega_0 t}, \quad n = 0, \pm1, \pm2, \ldots, \tag{B2}$$

where

$$c_n = \frac{1}{T}\int_{-\frac{T}{2}}^{\frac{T}{2}} f(t) e^{-in\omega_0 t}\mathrm{d}t. \tag{B3}$$

Therefore, the Fourier coefficient G_m of $d(z)$ is calculated as follows:

$$\begin{aligned} G_m &= \frac{1}{\Lambda}\int_{-\frac{\Lambda}{2}}^{\frac{\Lambda}{2}} \text{sign}[\cos(2\pi z/\Lambda)] e^{-i\frac{2\pi m}{\Lambda}z}\mathrm{d}z \\ &= \frac{1}{\Lambda}\int_{-\frac{\Lambda}{2}}^{-\frac{\Lambda}{4}} (-1) e^{-i\frac{2\pi m}{\Lambda}z}\mathrm{d}z + \frac{1}{\Lambda}\int_{-\frac{\Lambda}{4}}^{\frac{\Lambda}{4}} (1) e^{-i\frac{2\pi m}{\Lambda}z}\mathrm{d}z \\ &\quad + \frac{1}{\Lambda}\int_{\frac{\Lambda}{4}}^{\frac{\Lambda}{2}} (-1) e^{-i\frac{2\pi m}{\Lambda}z}\mathrm{d}z \\ &= \frac{1}{i2\pi m}\left[4i\,\sin\left(\frac{\pi m}{2}\right) - 2i\,\sin(\pi m)\right] \\ &= \frac{2}{m\pi}\,\sin\left(\frac{m\pi}{2}\right) \\ &= \text{sinc}\left(\frac{m\pi}{2}\right). \end{aligned} \tag{B4}$$

Now, we obtained the value of G_m in Eq. (5) of the main text.

Additionally, $d(z)$ can also be expressed in the form of a square wave.

For $|z| < \frac{\Lambda}{2}$,

$$d(z) = d_{\text{eff}} \cdot \left[2\,\text{rect}\left(\frac{2z}{\Lambda}\right) - 1\right]; \tag{B5}$$

and for $|\frac{\Lambda}{2}| < |z| < |\frac{L}{2}|$ (L is the length of crystal),

$$d(z) = d(z + m\Lambda), \quad m = 0, \pm1, \pm, 2, \ldots. \tag{B6}$$

We note that Eq. (5) can be intuitively understood as the Fourier transform of a square-wave function to a sinc function.

Acknowledgements

We thank Prof. Zhi-Yuan Zhou for helpful discussion. This work was supported by the National Natural Science Foundation of China (Nos. 12074299, 11704290, and 92365106), the Guangdong Provincial Key Laboratory (No. GKLQSE202102), and the Natural Science Foundation of Hubei Province (2022CFA039).

References

1. A. Anwar, C. Perumangatt, F. Steinlechner, *et al.*, "Entangled photon-pair sources based on three-wave mixing in bulk crystals," Rev. Sci. Instrum. **92**, 041101 (2021).
2. K. Zhang, S. Liu, Y. Chen, *et al.*, "Optical quantum states based on hot atomic ensembles and their applications," Photon. Insights **1**, R06 (2022).
3. A. Christ, A. Fedrizzi, H. Hübel, *et al.*, "Parametric down-conversion," in *Experimental Methods in the Physical Sciences*, A. Migdall ed. (Elsevier, 2013), p. 351.
4. C. Zhang, Y.-F. Huang, B.-H. Liu, *et al.*, "Spontaneous parametric down-conversion sources for multiphoton experiments," Adv. Quantum Technol. **4**, 2000132 (2021).
5. C. L. Morrison, F. Graffitti, P. Barrow, *et al.*, "Frequency-bin entanglement from domain-engineered down-conversion," APL Photonics **7**, 066102 (2022).
6. J.-L. Zhu, W.-X. Zhu, X.-T. Shi, *et al.*, "Design of mid-infrared entangled photon sources using lithium niobate," J. Opt. Soc. Am. B **40**, A9 (2023).

7. V. G. Dmitriev, G. G. Gurzadyan, and D. N. Nikogosyan, *Handbook of Nonlinear Optical Crystals*, Vol. **64** of Springer Series in Optical Sciences (Springer, 2013).
8. J. A. Nielsen, J. S. Neergaard-Nielsen, T. Gehring, *et al.*, "Deterministic quantum phase estimation beyond NOON states," Phys. Rev. Lett. **130**, 123603 (2023).
9. M. Reisner, F. Mazeas, R. Dauliat, *et al.*, "Quantum-limited determination of refractive index difference by means of entanglement," NPJ Quantum Inf. **8**, 58 (2022).
10. K. Hayama, B. Cao, R. Okamoto, *et al.*, "High-depth-resolution imaging of dispersive samples using quantum optical coherence tomography," Opt. Lett. **47**, 4949 (2022).
11. D. Tabakaev, M. Montagnese, G. Haack, *et al.*, "Energy-time-entangled two-photon molecular absorption," Phys. Rev. A **103**, 033701 (2021).
12. Y. Chen, S. Ecker, L. Chen, *et al.*, "Temporal distinguishability in Hong-Ou-Mandel interference for harnessing high-dimensional frequency entanglement," NPJ Quantum Inf. **7**, 167 (2021).
13. J. Yin, Y. Cao, Y.-H. Li, *et al.*, "Satellite-based entanglement distribution over 1200 kilometers," Science **356**, 1140 (2017).
14. H.-S. Zhong, H. Wang, Y.-H. Deng, *et al.*, "Quantum computational advantage using photons," Science **370**, 1460 (2020).
15. A. Lyons, G. C. Knee, E. Bolduc, *et al.*, "Attosecond-resolution Hong-Ou-Mandel interferometry," Sci. Adv. **4**, eaap9416 (2018).
16. Y. Guo, Z.-X. Yang, Z.-Q. Zeng, *et al.*, "Comparison of multi-mode Hong-Ou-Mandel interference and multi-slit interference," Opt. Express **31**, 32849 (2023).
17. K. Edamatsu, R. Shimizu, W. Ueno, *et al.*, "Photon pair sources with controlled frequency correlation," Prog. Inform. **8**, 19 (2011).
18. F. Graffitti, P. Barrow, A. Pickston, *et al.*, "Direct generation of tailored pulse-mode entanglement," Phys. Rev. Lett. **124**, 053603 (2020).
19. H. J. Lee, H. Kim, M. Cha, *et al.*, "Simultaneous type-0 and type-II spontaneous parametric down-conversions in a single periodically poled $KTiOPO_4$ crystal," Appl. Phys. B **108**, 585 (2012).
20. F. Steinlechner, M. Gilaberte, M. Jofre, *et al.*, "Efficient heralding of polarization-entangled photons from type-0 and type-II spontaneous parametric downconversion in periodically poled $KTiOPO_4$," J. Opt. Soc. Am. B **31**, 2068 (2014).
21. J. Chen, A. J. Pearlman, A. Ling, *et al.*, "A versatile waveguide source of photon pairs for chip-scale quantum information processing," Opt. Express **17**, 6727 (2009).
22. F. Laudenbach, S. Kalista, M. Hentschel, *et al.*, "A novel single-crystal single-pass source for polarisation- and colour-entangled photon pairs," Sci. Rep. **7**, 7235 (2017).
23. T. Y. Fan, C. E. Huang, B. Q. Hu, *et al.*, "Second harmonic generation and accurate index of refraction measurements in flux-grown $KTiOPO_4$," Appl. Opt. **26**, 2390 (1987).
24. K. Fradkin, A. Arie, A. Skliar, *et al.*, "Tunable midinfrared source by difference frequency generation in bulk periodically poled $KTiOPO_4$," Appl. Phys. Lett. **74**, 914 (1999).
25. S. Emanueli and A. Arie, "Temperature-dependent dispersion equations for $KTiOPO_4$ and $KTiOAsO_4$," Appl. Opt. **42**, 6661 (2003).
26. R. W. Boyd, *Nonlinear Optics* (Academic Press, 2020).
27. S. Niu, Z. Zhou, J. Cheng, *et al.*, "Multi-color laser generation in periodically poled KTP crystal with single period," Chin. Opt. Lett. **21**, 021901 (2023).
28. S.-J. Niu, C. Yang, Y. Li, *et al.*, "Cavity-enhanced frequency doubling with a third-order quasi-phase-matched PPKTP crystal," J. Opt. Soc. Am. B **38**, 2775 (2021).
29. N. Cai, W.-H. Cai, S. Wang, *et al.*, "Broadband-laser-diode pumped periodically poled potassium titanyl phosphate-sagnac polarization-entangled photon source," J. Opt. Soc. Am. B **39**, 77 (2022).
30. R.-B. Jin, R. Shimizu, K. Wakui, *et al.*, "Widely tunable single photon source with high purity at telecom wavelength," Opt. Express **21**, 10659 (2013).
31. Z. Zhang, C. Yuan, S. Shen, *et al.*, "High-performance quantum entanglement generation via cascaded second-order nonlinear processes," NPJ Quantum Inf. **7**, 123 (2021).
32. S. Shen, C. Yuan, Z. Zhang, *et al.*, "Hertz-rate metropolitan quantum teleportation," Light Sci. Appl. **12**, 115 (2023).
33. A. Fedrizzi, T. Herbst, A. Poppe, *et al.*, "A wavelength-tunable fiber-coupled source of narrowband entangled photons," Opt. Express **15**, 15377 (2007).
34. Y.-C. Liu, D.-J. Guo, R. Yang, *et al.*, "Narrowband photonic quantum entanglement with counterpropagating domain engineering," Photonics Res. **9**, 1998 (2021).
35. L. Hong, Y. Zhang, Y. Chen, *et al.*, "Fast quantifier of high-dimensional frequency entanglement through Hong–Ou–Mandel interference," Adv. Quantum Technol. **6**, 2300012 (2023).
36. J. Yin, Y. Cao, Y.-H. Li, *et al.*, "Satellite-based entanglement distribution over 1200 kilometers," Science **356**, 1140 (2017).
37. Y.-C. Jeong, K.-H. Hong, and Y.-H. Kim, "Bright source of polarization-entangled photons using a PPKTP pumped by a broadband multi-mode diode laser," Opt. Express **24**, 1165 (2016).
38. A. Lohrmann, C. Perumangatt, A. Villar, *et al.*, "Broadband pumped polarization entangled photon-pair source in a linear beam displacement interferometer," Appl. Phys. Lett. **116**, 021101 (2020).
39. N. Cai, W.-H. Cai, S. Wang, *et al.*, "Broadband-laser-diode pumped periodically poled potassium titanyl phosphate-Sagnac polarization-entangled photon source," J. Opt. Soc. Am. B **39**, 77 (2021).
40. Z.-X. Yang, Z.-Q. Zeng, Y. Tian, *et al.*, "Spatial–spectral mapping to prepare frequency entangled qudits," Opt. Lett. **48**, 2361 (2023).
41. W. Wang, K. Zhang, and J. Jing, "Large-scale quantum network over 66 orbital angular momentum optical modes," Phys. Rev. Lett. **125**, 140501 (2020).
42. K. Zhang, W. Wang, S. Liu, *et al.*, "Reconfigurable hexapartite entanglement by spatially multiplexed four-wave mixing processes," Phys. Rev. Lett. **124**, 090501 (2020).
43. H. Vanherzeele and J. D. Bierlein, "Magnitude of the nonlinear-optical coefficients of $KTiOPO_4$," Opt. Lett. **17**, 982 (1992).
44. C. Lanczos and J. Boyd, *Discourse on Fourier Series* (SIAM, 2016).